Constitutive modelling of ductile damage matrix reinforced by platelets-like particles with imperfect interfaces: Application to graphene polymer nanocomposite materials

Wiyao Azoti*, Ahmed Elmarakbi

Automotive Composites Group, Faculty of Engineering and Advanced Manufacturing, University of Sunderland, SR6 0DD, UK

Abstract

In this paper, the mechanical response of composites consisting of ductile matrix reinforced by platelets-like particles is derived with imperfect interfaces. Due to its flexibility to study imperfect interfaces with limited number of model parameters, the linear spring model LSM is considered. Moreover, the interfacial contribution to the strain concentration tensor within each material phase and inside the average strain filed is described by a modified Mori-Tanaka scheme. The material nonlinearity is established by the J_2 plasticity and Lemaitre-Chaboche damage model. A generalised mid-point rule is used to solve rate equations yielding to anisotropic consistent (algorithmic) tangent operators. To avoid spurious macroscopic stress-strain response, an isotropisation procedure is adopted during the computation of a modified Eshelby's tensor. Numerical results are performed on graphene platelets GPL-reinforced polymer PA6 composite. They confirm the possibility to achieve high stiffness with low values of GPL aspect ratio. The accumulated plastic strain and the damage variable within the matrix are influenced by the GPL volume fraction which is also involved in the softening of the overall response when imperfection is considered at the interface.

Keywords: Interface, Graphene platelets, Ductile damage, Algorithmic tangent operators, Micromechanics

1. Introduction

Platelets-like particles represent a type of ellipsoidal oblate inclusions that are characterised by a very small thickness compared to both others semi-axis dimensions. Platelets-like particles become attractive with the development of nanocomposites such as the graphene platelets GPL based polymer composites. It is reported [1] substantial property enhancements at much lower

*Corresponding author. Tel. +44 191 515 2684
Email address: Wiyao.Azoti@sunderland.ac.uk (Wiyao Azoti)

volume fraction with respect to polymer composites containing conventional micron-scale fillers (such as glass or carbon fibres). For deriving properties at the nanoscale, analysis accounting for the size dependent effect have been performed [2]. In addition, multi scale analyses combining molecular mechanics theories and continuum models have been developed for graphene polymer composites. The graphene properties are often derived at atomistic scale and the nano particles are treated as equivalent continuum particles [3, 4] that are embedded in the polymer matrix through conventional homogenisation techniques.

Despite graphene has been used to increase stiffness, toughness and thermal conductivity of polymer resins by a large margin [5–8], there are still much technological challenges to overcome mainly in the material modelling. This is characterised by the lack of sufficient knowledge on graphene composites for structural applications describing interfacial properties between graphene and polymer matrix under severe loading conditions. It is well-known that the interface characterises the load transfer between the particles/fibres and the matrix. It can significantly change the overall properties. Several micromechanics models have been developed for accounting for the properties of the interface. Among them, one can distinguish the interphase models [9–13] as well as interface models [14–23]. The latter i.e the interface models introduce discontinuites in the displacement and/or stress fields at the interface. Among them, is there the linear spring model LSM (Hashin [24, 25], Qu [26, 27], Zhong and Meguid [28]). Springs like zero-thickness interface model based on bilateral, independent elastic springs has been developed by Mancusi et al. [29] to study the influence of the debonding in the torsional strengthening and the local interactions between a reinforced concrete beams and layers of fibre-reinforced composite reinforcement. Works by Ascione et al. [30] to predict the actual stress state at the interface between concrete core and reinforcing plate should be cited. Herein, LSM is very attractive for its simplicity and flexibility to treat imperfect interface with limited number of model parameters [31].

In this work, LSM is considered to analyse the effect of an imperfect interface on the ductile damage response of GPL nanocomposite materials. GPL are considered as continuum phases interacting with the polymer matrix through a slightly weakened interface. The solution of the heterogeneous material problem is obtained by the kinematic integral equation of Dederichs and Zeller [32]. The non linear framework, which is that recently used by Tchalla et al. [33], is based on a Hill-type incremental formulation with the classical J_2 flow rule. For the matrix phase, the damage behaviour is introduced through the so-called effective stress $\hat{\boldsymbol{\sigma}}$. The damage variable D undergoes Lemaitre and Chaboche's ductile law. Following works of Doghri [34], the algorithmic (consistent) modulus is obtained for the ductile matrix. By accounting for the contribution of

the interface, on the one hand inside the strain concentration tensor of the inclusions through the modified Eshelby's tensor [26, 27], and on the other hand in the average strain field , a modified version of the Mori-Tanaka is derived for the effective properties. The well-known damage localisation problem is not addressed herein. Works dealing with such issues are based on non-local approaches. An implicit gradient-enhanced approach has been used by Wu et al. [35, 36] to study the non-linear behaviour of ductile damage matrix composites with the strain/damage localisation due to the loss of solution uniqueness. Besides, a gradient non-local approach has been formulated for treating a softening behaviour of nanobeams by Barretta et al. [37] and Apuzzo et al. [38] while analytical based finite element formulations accounting for the nonlocal interactions between elastic heterogeneities at microscopic level have been also provided by Barretta et al. [39]. In this work, critical loadings reaching the lost of uniqueness are avoided in applications by checking the positive-definite properties of the algorithmic modulus. Next, the modified Eshelby's tensor involved in the global strain concentration is computed by an isotropisation of the matrix algorithmic modulus. This isotropisation discussed in Doghri and Ouaar [40] and Chaboche et al. [41] is essential to avoid spurious stiff macro stress-strain responses.

The paper is organised as follows: section 2 establishes the fundamentals of a micromechanics homogenisation by deriving the global strain concentration tensor; in section 3, the algorithmic tangent operator, derived from the Chaboche's ductile damage, is recalled. Section 4 gives expressions of the imperfect interface in terms of traction and displacements as well as the modified Eshelby's tensor while section 5 derives the modified Mori-Tanaka scheme for overall responses. The algorithm for deriving the overall properties is presented in section 6. Finally, the model predictions are therefore compared with open literature data in section 7 where a systematic analysis of micro parameters (aspect ratio, volume fraction, interfacial compliance) is carried out for a GPL-reinforced polymer PA6 under uniaxial tests.

2. Fundamentals of Micromechanics

2.1. Kinematic integral equation

Let us consider a composite material consisting of $N+1$ phases. The matrix (phase 0) can be a specific constituent containing all remaining phases. To study this composite, a Representative Volume Element (RVE) is considered. On the RVE boundaries (Fig. 1), admissible macroscopic static or kinematic loads are applied in the absence of body forces and inertia terms. The micromechanics scale transition consists, firstly, in the localization of the macroscopic strain tensor

$\mathbf{E}$ through a fourth order global strain concentration tensor $\mathbf{A}(r)$ and, secondly, in the homogenization, which uses averaging techniques to approximate the macroscopic behaviour. Note that $\mathbf{A}(r)$ remains the unknown parameter that contains all the information about the microstructure. The effective properties of the RVE are given by:

$$\mathbf{C}^{eff} = \frac{1}{V}\int_V \mathbf{c}(r) : \mathbf{A}(r) dV \tag{1}$$

where $\mathbf{c}(r)$ denotes the local stiffness tensor and V the volume of the RVE. The operator ":" stands

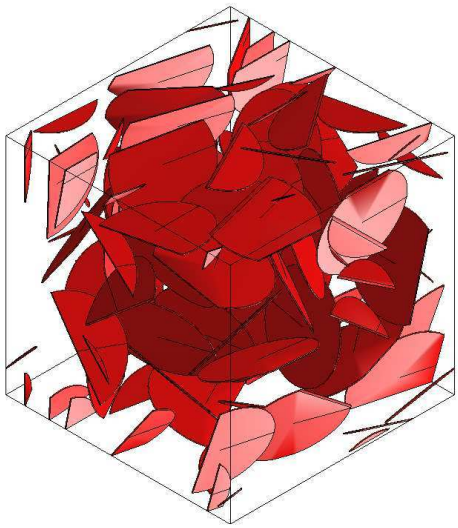

Figure 1: Illustration of platelets-like inclusions reinforced 3D random RVE.

for the tensorial contraction over two indices. The global strain concentration tensor $\mathbf{A}(r)$ links the local strain $\boldsymbol{\epsilon}(r)$ to the macroscopic strain $\mathbf{E}$ as follows:

$$\boldsymbol{\epsilon}(r) = \mathbf{A}(r) : \mathbf{E} \tag{2}$$

The decomposition of the local stiffness tensor into a homogeneous reference part $\mathbf{c}^R$ and a fluctuation part $\delta\mathbf{c}$ such as:

$$\mathbf{c}(r) = \mathbf{c}^R(r) + \delta\mathbf{c}(r) \tag{3}$$

Equation (3) enables the derivation of the kinematic integral equation of Dederichs and Zeller [32]. In terms of strain fields, the kinematic integral equation reads:

$$\boldsymbol{\epsilon}(r) = \mathbf{E}^R(r) - \int_V \boldsymbol{\Gamma}(r - r') : \delta\mathbf{c}(r') : \boldsymbol{\epsilon}(r') dV' \tag{4}$$

where $\mathbf{E}^R(r)$ is the strain field inside the reference infinite medium and $\boldsymbol{\Gamma}(r - r')$ is the modified Green tensor.

2.2. *Global strain concentration tensor*

The kinematic integral equation (4) represents the formal solution the global strain concentration tensor is derived from. Based on an iterative procedure proposed by Vieville et al. [42], the global strain concentration tensor $\mathbf{A}^I(r)$ for a I^{th} phase of the RVE is given as:

$$\begin{cases} \mathbf{A}^I(r) = \mathbf{a}^I(r) : (\bar{\mathbf{a}}^I(r))^{-1} \\ \bar{\mathbf{A}}^I(r) = \mathbf{I} \end{cases} \tag{5}$$

$\mathbf{I}$ represents the fourth order symmetric identity tensor and $\bar{\bullet}$ is the mean-field volume average of $\bullet$. The quantity $\mathbf{a}^I(r)$ is the local strain concentration tensor with respect to the reference medium such that:

$$\boldsymbol{\epsilon}^I(r) = \mathbf{a}^I(r) : \mathbf{E}^R \tag{6}$$

The I^{th} concentration tensor $\mathbf{a}^I$ is given by:

$$\begin{cases} \mathbf{a}_0^I(r) = \mathbf{I} \\ \mathbf{a}_{i+1}^I(r) = [\mathbf{I} + \mathbf{T}^{II} : (\mathbf{c}^I(r) - \mathbf{c}^R(r))]^{-1} : [\mathbf{I} - \sum_{J=0, J\neq I}^{N} \mathbf{T}^{IJ} : (\mathbf{c}^J(r) - \mathbf{c}^R(r)) : \mathbf{a}_i^J(r)] \\ I = 0, 1, 2, ..., N \end{cases} \tag{7}$$

with N the number of phases considered in the composite. In equation (7), $\mathbf{a}_i^I(r)$ represents an approximation of the I^{th} concentration tensor at iteration i. $\mathbf{T}^{II}$ and $\mathbf{T}^{IJ}$ are the interaction tensors in one-site (OS) and multi-site (MS) versions, respectively. Their general expression is:

$$\mathbf{T}^{IJ} = \frac{1}{V_I} \int_{V_I} \int_{V_J} \boldsymbol{\Gamma}(r - r') dV dV' \tag{8}$$

The computational framework of $\mathbf{T}^{II}$ and $\mathbf{T}^{IJ}$ is proposed by Fassi-Fehri [43].

Let us suppose that the geometry of any phase within the RVE is ellipsoidal. The Eshelby's inclusion concept [44] assumes that the strain field inside an ellipsoidal inclusion is uniform. Therefore, a characteristic function $\theta(r)$ can be defined such as [42]:

$$\theta(r) = \begin{cases} 1 & \text{if } r \in V_I \\ 0 & \text{if } r \notin V_I \end{cases} \tag{9}$$

Based on equation (9) and the average strain field within an inclusion I such as:

$$\boldsymbol{\epsilon}^I = \frac{1}{V_I} \int_{V_I} \boldsymbol{\epsilon}\left(\mathbf{r}\right) dV \tag{10}$$

the above kinematic integral equation (4) can be rewritten as:

$$\boldsymbol{\epsilon}^I = \mathbf{E}^R - \sum_{J=0}^{N} \mathbf{T}^{IJ} : (\mathbf{c}^J - \mathbf{c}^R) : \boldsymbol{\epsilon}^J \text{ with } I = 0, 1, 2, ..., N \tag{11}$$

and the local concentration tensor Eq.(7) becomes:

$$\begin{cases} \mathbf{a}_0^I = \mathbf{I} \\ \mathbf{a}_{i+1}^I = [\mathbf{I} + \mathbf{T}^{II}(\mathbf{c}^R) : (\mathbf{c}^I - \mathbf{c}^R)]^{-1} : [\mathbf{I} - \sum_{J=1, J\neq I}^{N} \mathbf{T}^{IJ} : (\mathbf{c}^J - \mathbf{c}^R) : \mathbf{a}_i^J] \\ I = 0, 1, 2, ..., N \end{cases} \tag{12}$$

In the case of OS version (most frequent developments in the literature) and for isotropic medium, the interaction tensor $\mathbf{T}^{II}$ can be deduced from the Eshelby's tensor $\mathbf{S}$ such as $\mathbf{T}^{II} = \mathbf{S} : (\mathbf{c}^R)^{-1}$. In such condition and neglecting the interactions among inclusion I and its neighbours J, i.e. all the tensors $\mathbf{T}^{IJ} = 0$, the local concentration tensor $\mathbf{a}^I$ reads more simple expression:

$$\mathbf{a}^I = [\mathbf{I} + \mathbf{S} : (\mathbf{c}^R)^{-1} : (\mathbf{c}^I - \mathbf{c}^R)]^{-1} \text{ with } I = 0, 1, 2, ..., N \tag{13}$$

Finally, the global strain concentration tensor $\mathbf{A}^I$ is calculated by substituting equation (13) in (5). Therefore, for any homogenization model defined by $\mathbf{A}^I$, the effective or macro-stiffness tensor $\mathbf{C}^{eff}$ is given through a discrete form of the equation (1) by:

$$\mathbf{C}^{eff} = \sum_{I=0}^{N} f_I \mathbf{c}^I : \mathbf{A}^I. \tag{14}$$

with the volume fraction f_I defined as:

$$f_I = \frac{V_I}{V} \tag{15}$$

3. Ductile damage-based non linear tangent operators

In this section, the "consistent" (algorithmic) $\mathbf{C}^{alg}$ tangent operator will be derived from a discretisation in the time interval $[t_n, t_{n+1}]$ of Hill-type rate constitutive equation. The damage is represented by a state internal variable D such as $(0 \leq D < 1)$ and based on the concept of effective stress $\hat{\boldsymbol{\sigma}}$. This latter characterises the undamaged representation of the RVE. It is seen as the tensor which resists to the load and yields:

$$\hat{\boldsymbol{\sigma}} = \frac{\boldsymbol{\sigma}}{1 - D} \tag{16}$$

In equation (16), $\boldsymbol{\sigma}$ represents the stress state accounting for the damage evolution. The differentiation of $\boldsymbol{\sigma}$ with respect to the total strain $\boldsymbol{\epsilon}$ leads to the "consistent" (algorithmic) $\mathbf{C}^{alg}$ tangent operator:

$$\delta\boldsymbol{\sigma}_{n+1} = \mathbf{C}^{alg} : \delta\boldsymbol{\epsilon}_{n+1} \tag{17}$$

3.1. Algorithmic (consistent) tangent operator $\mathbf{C}^{alg}$

Variables with subscript "$(\bullet)_{n+1}$" are computed at the current time increment and those with subscript "$(\bullet)_n$" are computed at the previous time increment. The J_2 flow rule accounting for Lemaitre-Chaboche damage is obtained by considering the following equations:

$$\begin{cases} \boldsymbol{\sigma} = (1-D)\mathbf{C}^{el} : (\boldsymbol{\epsilon} - \boldsymbol{\epsilon}^p) \\ f(\hat{\boldsymbol{\sigma}}, R, D) = J_2(\hat{\boldsymbol{\sigma}}) - R(r) - \sigma_Y \\ \dot{r} = (1-D)\dot{p} \text{ with } \dot{r} \geq 0 \text{ and } \dot{r} f = 0 \text{ and } \dot{r}\dot{f} = 0 \\ J_2(\hat{\boldsymbol{\sigma}}) = [\frac{3}{2}(\hat{\boldsymbol{s}}) : (\hat{\boldsymbol{s}})]^{1/2} \text{ with } \hat{\boldsymbol{s}} = \hat{\boldsymbol{\sigma}} - \left(\frac{1}{3}\right)(tr\hat{\boldsymbol{\sigma}})\,\mathbf{1} \\ \dot{\boldsymbol{\epsilon}}^p = \dot{p}\hat{\mathbf{N}} \text{ with } \dot{p} = \left(\frac{2}{3}\dot{\boldsymbol{\epsilon}}^p : \dot{\boldsymbol{\epsilon}}^p\right)^{1/2} \\ \hat{\mathbf{N}} = \frac{\partial f}{\partial \hat{\boldsymbol{\sigma}}} = \left(\frac{3}{2}\right)\frac{\hat{s}}{J_2(\hat{\boldsymbol{\sigma}})} \\ \dot{D} = (\frac{\mathbf{Y}}{S_0})^s \dot{p} \text{ if } p \geq p_c \text{ and } D \leq D_c \end{cases} \tag{18}$$

where, $\mathbf{C}^{el}$ denotes the material elastic stiffness tensor while $\boldsymbol{\epsilon}$ and $\boldsymbol{\epsilon}^p$ are the total and plastic strains, respectively. The yield function $f(\hat{\boldsymbol{\sigma}}, R, D)$ establishes the yield surface in which σ_Y is the initial yield stress and $R(r)$ the hardening stress with $\dot{r}$ the plastic multiplier variable and p the accumulated plastic strain. $\hat{\mathbf{N}}$ represents the normal to the yield surface in stress space whereas $\hat{\boldsymbol{s}}$ is the deviatoric stress and $\mathbf{1}$ the second order symmetric identity tensor. $\mathbf{Y}$ represents the rate of damage strain energy release. S_0 and s are material parameters. In order to obtain the algorithmic tangent operator $\mathbf{C}^{alg}$, a first step consists to solve the effective algorithmic tangent operator $\hat{\mathbf{C}}^{alg}$ given by:

$$\delta\hat{\boldsymbol{\sigma}}_{n+1} = \hat{\mathbf{C}}^{alg} : \delta\boldsymbol{\epsilon}_{n+1} \tag{19}$$

The general framework for the derivation of $\hat{\mathbf{C}}^{alg}$ is set up by Doghri in [34]. In this paper, we use the classical equations leading to the effective tangent operator $\hat{\mathbf{C}}^{alg}$ given by:

$$\begin{cases} \hat{\mathbf{C}}^{alg} = \hat{\mathbf{C}}^{ep} - (2G)^2 \frac{\Delta p}{[1+(3/2)g]} \frac{\partial^2 f}{\partial\hat{\boldsymbol{\sigma}}\partial\hat{\boldsymbol{\sigma}}} \\ \hat{\mathbf{C}}^{ep} = \mathbf{C}^{el} - (2G)^2 \frac{\hat{\mathbf{N}}\otimes\hat{\mathbf{N}}}{h} \\ h = 3G + \frac{\partial R}{\partial r} \end{cases} \tag{20}$$

where G denotes the material shear modulus and the operator "$\otimes$" designates the tensor product. The parameter g and tensor $\frac{\partial^2 f}{\partial\hat{\boldsymbol{\sigma}}\partial\hat{\boldsymbol{\sigma}}}$ are given by:

$$\begin{cases} g = \frac{1}{J_2(\hat{\boldsymbol{\sigma}})}(2G\Delta p) > 0 \\ \frac{\partial^2 f}{\partial\hat{\boldsymbol{\sigma}}\partial\hat{\boldsymbol{\sigma}}} = \frac{1}{J_2(\hat{\boldsymbol{\sigma}})}\left(\frac{3}{2}\mathbf{I}^{dev} - \hat{\mathbf{N}}\otimes\hat{\mathbf{N}}\right) \end{cases} \tag{21}$$

with $\mathbf{I}^{dev}$ the deviatoric part of the fourth order symmetric identity tensor. A new shortened notation y is introduced. The damage strain energy release $\mathbf{Y}$ is given by:

$$\begin{cases} y = \left(\frac{\mathbf{Y}}{S_0}\right)^s \\ \mathbf{Y} = \frac{1}{2E}\left[\frac{J_2(\hat{\boldsymbol{\sigma}})}{1-D}\right]^2 \mathbf{R}_v \\ \mathbf{R}_v = \frac{2}{3}(1+\nu) + 3(1-2\nu)\left[\frac{\hat{\boldsymbol{\sigma}}_H}{J_2(\hat{\boldsymbol{\sigma}})}\right]^2 \text{ with } \hat{\boldsymbol{\sigma}}_H = \frac{\hat{\boldsymbol{\sigma}}_{kk}}{3} \end{cases} \tag{22}$$

The algorithmic tangent operator $\mathbf{C}^{alg}$ is therefore obtained from the effective algorithmic tangent operator computed from equations (20)-(22). Its expression yields :

$$\mathbf{C}^{alg} = (1-D)\hat{\mathbf{C}}^{alg} \tag{23}$$

Equation (23) corresponds to the local stiffness tensor of the material's constituent. It will be used in section 5 for homogenisation purposes. It depends of some internal variables such as (r, p, D).

3.2. Internal variables computation: Return mapping algorithm

The statement of the problem in a time interval $[t_n, t_{n+1}]$ is the following: when the solution in terms of $(\boldsymbol{\sigma}, \boldsymbol{\epsilon}, r, p, D)$ is known at t_n, a given applied strain increment (load) at t_{n+1} must lead to the solution at t_{n+1}. Note that the known variable of the problem is the applied strain increment $\Delta\boldsymbol{\epsilon}$. An increment is defined such as:

$$\Delta(\bullet) = (\bullet)_{n+1} - (\bullet)_n \tag{24}$$

The first equation of system (18) can be rewritten at time t_{n+1} as follow [34]:

$$\boldsymbol{\sigma}_{n+1} = (1-D_{n+1})\mathbf{C}^{el} : [(\boldsymbol{\epsilon}_n + \Delta\boldsymbol{\epsilon}) - (\boldsymbol{\epsilon}_n^p + \Delta\boldsymbol{\epsilon}^p)] \tag{25}$$

At the beginning of the time interval t_n, the response of the loaded material is considered purely elastic, therefore $\Delta p = 0, \Delta\boldsymbol{\epsilon}^p = 0, \Delta D = 0$. This state called "the elastic predictor" yields in terms of stress at time t_{n+1}:

$$\hat{\boldsymbol{\sigma}}_{n+1}^{trial} = \mathbf{C}^{el} : (\boldsymbol{\epsilon}_{n+1} - \boldsymbol{\epsilon}_n^p) \text{ and } \boldsymbol{\sigma}_{n+1}^{trial} = (1-D_n)\hat{\boldsymbol{\sigma}}_{n+1}^{trial} \tag{26}$$

- if $\hat{\boldsymbol{\sigma}}_{n+1}^{trial}$ satisfies the flow rule such as $f_{n+1}^{trial} = J_2(\hat{\boldsymbol{\sigma}}_{n+1}^{trial}) - R(r_n) - \sigma_Y \leq 0$, therefore the solution is given by:

$$\begin{cases} \hat{\boldsymbol{\sigma}}_{n+1} = \hat{\boldsymbol{\sigma}}_{n+1}^{trial} \text{ and } \boldsymbol{\sigma}_{n+1} = (1-D_n)\hat{\boldsymbol{\sigma}}_{n+1} \\ \left(r_{n+1}, p_{n+1}, D_{n+1}, \boldsymbol{\epsilon}_{n+1}^p\right) = (r_n, p_n, D_n, \boldsymbol{\epsilon}_n^p) \end{cases} \tag{27}$$

- else if $\hat{\boldsymbol{\sigma}}_{n+1}^{trial}$ does not satisfy the flow rule i.e $f_{n+1}^{trial} = J_2(\hat{\boldsymbol{\sigma}}_{n+1}^{trial}) - R(r_n) - \sigma_Y > 0$, then the plasticity occurs and the solution must be corrected (plastic corrector) so that $f_{n+1} = 0$ is satisfied. This implies to find $\hat{\boldsymbol{\sigma}}_{n+1}$ such as:

$$\hat{\boldsymbol{\sigma}}_{n+1} = \hat{\boldsymbol{\sigma}}_{n+1}^{trial} - \mathbf{C}^{el} : \Delta\boldsymbol{\epsilon}^p \tag{28}$$

which can be rewritten, by taken into account the deviatoric nature of $\Delta\boldsymbol{\epsilon}^p$, as:

$$\hat{\boldsymbol{\sigma}}_{n+1} = \hat{\boldsymbol{\sigma}}_{n+1}^{trial} - 2G\Delta\boldsymbol{\epsilon}^p \tag{29}$$

The unknown plastic strain increment $\Delta\boldsymbol{\epsilon}^p$ in equation (29) is evaluated by solving the following non linear system of equations:

$$\begin{cases} k_{\hat{\boldsymbol{\sigma}}} = \hat{\boldsymbol{\sigma}} - \hat{\boldsymbol{\sigma}}^{trial} + 2G\Delta\boldsymbol{\epsilon}^p = 0 \\ k_f = J_2(\hat{\boldsymbol{\sigma}}) - R(r) - \sigma_Y = 0 \\ k_D = \Delta D - y(\hat{\boldsymbol{\sigma}})\frac{\Delta r}{1-D} = 0 \end{cases} \tag{30}$$

Newton-Raphson technique is used to solve the above non-linear equations (30). More technical details about this resolution can be found in [34].

Once the iterative procedure converges, the internal variables $r_{n+1}, p_{n+1}, D_{n+1}$ and the effective stress $\hat{\boldsymbol{\sigma}}_{n+1}$are known. Therefore, the algorithmic tangent operator equation (23) can be fully determined and the micromechanics approach can now be addressed for the composite material. A detailed procedure about internal variables computation can be found in [45].

4. Imperfect interface and the modified Eshelby's tensor

Let us consider the interface γ between two phases of a composite material. The linear spring model LSM supposes the continuity of the traction vector across the interface while the jump of displacment field is consedered to be proportional to the traction on that interface. These assumption are written like:

$$\begin{cases} \Delta\sigma_{ij}n_j = \left[\sigma_{ij}\left(\gamma^+\right) - \sigma_{ij}\left(\gamma^-\right)\right]n_j = 0 \\ \Delta u_i = \left[u_i\left(\gamma^+\right) - u_i\left(\gamma^-\right)\right] = \eta_{ij}\sigma_{jk}n_k \end{cases} \tag{31}$$

with n_j the components of a unit vector normal to the interface. $u_i\left(\gamma^+\right)$ and $u_i\left(\gamma^-\right)$ stand for the values of $u_i\left(x\right)$ as x reaches the interface from outside and inside of the inclusion respectively. $\sigma_{ij}\left(\gamma^+\right)$ and $\sigma_{ij}\left(\gamma^-\right)$ are the dual in terms of stress. The second order tensor components η_{ij} denote the compliance of the interface. It appears that $\eta_{ij} = 0$ leads to a perfectly bonded interface

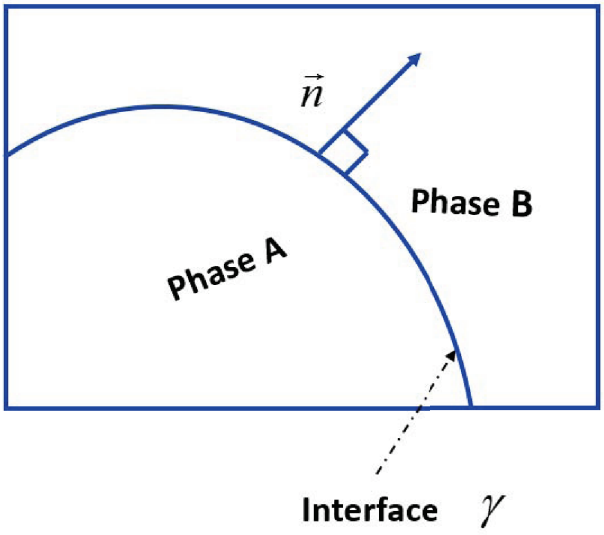

Figure 2: Illustration of the interface around 2-phases of a composite.

whereas $\eta_{ij} \longrightarrow \infty$ represents a completely debonded interface. The expression of η_{ij} is given by [26, 27]:

$$\eta_{ij} = \alpha\delta_{ij} + (\beta - \alpha)\, n_i n_j \tag{32}$$

where the constants α and β stand for the extent of interfacial sliding and the interfacial separation, respectively. δ_{ij} is the Kronecker symbol. In the case of ellipsoidal inclusions, Qu [26, 27] has determined the Eshelby's tensor for these inclusions embedded in an elastic matrix and showing a slightly weakened interface i.e when η_{ij} is very small. Therefore, the modified Eshelby's tensor for this problem yields :

$$\mathbf{S^M} = \mathbf{S} + (\mathbf{I} - \mathbf{S}) : \mathbf{H} : \mathbf{c} : (\mathbf{I} - \mathbf{S}) \tag{33}$$

where $\mathbf{S}$ denotes the original Eshelby's tensor [44] and $\mathbf{H}$ stands for a four order tensor depending on the interface properties and the geometry of the inclusion. Expressions of $\mathbf{H}$ for ellipsoidal inclusions are given in Appendix A. In others terms, Eq. (33) can be written such as:

$$S^{\mathbf{M}}_{ijkl} = S_{ijkl} + (I_{ijpq} - S_{ijpq})\, H_{pqrs} c_{rsmn}\, (I_{mnkl} - S_{mnkl}) \tag{34}$$

5. Modified Mori-Tanaka scheme for overall responses

General considerations on Mori-Tanaka scheme can be found in works by Azoti et al. [46]. Therefore, the MT effective properties are given by:

$$\mathbf{C^{MT}} = \sum_{I=0}^{N} f_I \mathbf{c}^I : \mathbf{A}^I = (f_0 \mathbf{c}^0 + \sum_{J=1}^{N} f_I \mathbf{c}^I : \mathbf{a}^I) : \mathbf{A}^0 \tag{35}$$

with $\mathbf{A}^0$ the global strain concentration of the matrix. By accounting for the interface contributions, modifications come out with the definition of the average strain field:

$$\mathbf{E} = \frac{1}{V}\int_V \boldsymbol{\epsilon}\left(\mathbf{x}\right) dV = \sum_{I=0}^{N} f_I \boldsymbol{\epsilon}^I + \frac{1}{V}\int_\gamma \frac{1}{2}\left(\Delta\mathbf{u}\otimes\mathbf{n} + \mathbf{n}\otimes\Delta\mathbf{u}\right)dS \tag{36}$$

where γ represents the union of all interfaces. The combination of Eq.(31)-b and Eq.(36) leads to the following expression of the average strain:

$$\mathbf{E} = \sum_{I=0}^{N} f_I \boldsymbol{\epsilon}^I + \frac{1}{V}\sum_{I=1}^{N}\int_{\gamma_I} \frac{1}{2}\left[\left(\boldsymbol{\eta}.\boldsymbol{\sigma}.\mathbf{n}\right)\otimes\mathbf{n} + \mathbf{n}\otimes\left(\boldsymbol{\eta}.\boldsymbol{\sigma}.\mathbf{n}\right)\right]dS \tag{37}$$

with γ_I the surface of the volume V_I.

The evaluation of the integral terms in Eq.(37) remains tricky for an arbitrary interface geometry. However by taking advantage of developments by Qu [26] for slightly weakened interface, the stress distribution on the surface γ_I can be replaced by its average over the volume V_I leading to a simplified form of Eq.(37) such as:

$$\mathbf{E} = \sum_{I=0}^{N} f_I \boldsymbol{\epsilon}^I + \sum_{I=1}^{N} f_I \mathbf{H}^I : \boldsymbol{\sigma}^I \tag{38}$$

Using Eq.(5) and derivations in [46], one can demonstrate the following relationship between the average strain within an inclusion and the matrix such as:

$$\boldsymbol{\epsilon}^I = \mathbf{a}^I : \boldsymbol{\epsilon}^0 \tag{39}$$

where $\mathbf{a}^I$ in the OS-version yields:

$$\mathbf{a}^I = \left[\mathbf{I} + \mathbf{S}^{\mathbf{M}} : \left(\mathbf{c}^R\right)^{-1} : \left(\mathbf{c}^I - \mathbf{c}^R\right)\right]^{-1} \text{ with } I = 1, 2, ..., N \tag{40}$$

Combining Eq.(39) and Eq.(38) leads to

$$\mathbf{E} = \left[\sum_{I=0}^{N} f_I \mathbf{a}^I + \sum_{I=1}^{N} f_I \mathbf{H}^I : \mathbf{c}^I : \mathbf{a}^I\right] : \boldsymbol{\epsilon}^0 \tag{41}$$

The inversion of Eq.(38)

$$\boldsymbol{\epsilon}^0 = \left[\sum_{I=0}^{N} f_I \mathbf{a}^I + \sum_{I=1}^{N} f_I \mathbf{H}^I : \mathbf{c}^I : \mathbf{a}^I\right]^{-1} : \mathbf{E} \tag{42}$$

in conjunction with Eq.(2) leads to the modified global concentration tensor of the matrix $\mathbf{A}^0$ such as:

$$\mathbf{A}^0 = \left[\sum_{I=0}^{N} f_I \mathbf{a}^I + \sum_{I=1}^{N} f_I \mathbf{H}^I : \mathbf{c}^I : \mathbf{a}^I\right]^{-1} \tag{43}$$

Substituting Eq.(43) into Eq.(35) gives the modified Mori-Tanaka effective properties such as:

$$\mathbf{C}^{\mathbf{MT}}_{modified} = \left(f_0\mathbf{c}^0 + \sum_{I=1}^{N} f_I\mathbf{c}^I : \mathbf{a}^I \right) : \left[\sum_{I=0}^{N} f_I : \mathbf{a}^I + \sum_{I=1}^{N} f_I\mathbf{H}^I : \mathbf{c}^I : \mathbf{a}^I \right]^{-1} \tag{44}$$

In the case a 2-phase composite, Eq.(44) yields

$$\mathbf{C}^{\mathbf{MT}}_{modified} = \left(f_0\mathbf{c}^0 + f_I\mathbf{c}^I : \mathbf{a}^I\right) : \left[f_0\mathbf{I} + f_I\left(\mathbf{I} + \mathbf{H}^I : \mathbf{c}^I\right) : \mathbf{a}^I\right]^{-1} \tag{45}$$

6. Algorithm for solving the homogenised ductile damage responses

For a time $[t_n, t_{n+1}]$ increment, the input variables of the problem are: the macro strain $\mathbf{E}_n$ at t_n and the macro strain increment $\Delta\mathbf{E}$ such as $\mathbf{E}_{n+1} = \mathbf{E}_n + \Delta\mathbf{E}$. The output variable is the macrostress such as $\mathbf{\Sigma}_{n+1} = \mathbf{\Sigma}_n + \Delta\mathbf{\Sigma}$. The following steps summarise the constitutive algorithm presented in Figure 3.

1. Initialization of the strain increment in the inclusions phase: $\Delta\boldsymbol{\epsilon}^I = \mathbf{A}^I : \Delta\mathbf{E}$ such as $\mathbf{A}^I = \mathbf{I}$
   - Update the stress in inclusions phase from equations (27) or (30);
   - Compute the inclusions algorithmic moduli $\mathbf{C}_I^{alg}$ using equation (23).
2. Compute the strain increment in the matrix phase: $\Delta\boldsymbol{\epsilon}^0 = \frac{\Delta\mathbf{E} - f_I\Delta\boldsymbol{\epsilon}^I}{1-f_I}$
   - Update the stress in the matrix phase from equations (27) or (30);
   - Compute the matrix algorithmic moduli $\mathbf{C}_0^{alg}$ using equation (23).
3. Apply the mid-point rule at time $t_{n+\alpha}$ to the algorithmic moduli of the inclusions and the matrix (see [40]):
   - $[\mathbf{C}_0^{alg}]_{n+\alpha} = (1-\alpha)[\mathbf{C}_0^{alg}]_n + \alpha[\mathbf{C}_0^{alg}]_{n+1}$;
   - $[\mathbf{C}_I^{alg}]_{n+\alpha} = (1-\alpha)[\mathbf{C}_I^{alg}]_n + \alpha[\mathbf{C}_I^{alg}]_{n+1}$;
   - $\alpha \in [0,1]$. (Here $\alpha = \frac{1}{2}$ is used)
4. Compute the global strain concentration tensor $\mathbf{A}^I = \mathbf{a}^I : \mathbf{A}^0$ from equation (40) and (43) using the modified Mori-Tanaka scheme
5. Calculate the residual
   - $R = \mathbf{A}^I : \Delta\mathbf{E} - \Delta\boldsymbol{\epsilon}^I$;
6. If $|R| \leq \mathbf{TOL} = 10^{-8}$, then exit the loop and go to the step 8

7. else Go to step 1 using the computed value of the global strain concentration tensor $\mathbf{A}^I$
8. Compute the homogenised tangent properties $\mathbf{C}^{\mathbf{MT}}_{modified}$ from equation (44) and based on anisotropic moduli in step 3
9. Finally, compute the macroscopic stress increment
   - $\Delta\boldsymbol{\Sigma} = \mathbf{C}^{\mathbf{MT}}_{modified} : \Delta\mathbf{E}$;

The above steps describing the algorithm is represented in the Figure 3.

7. Numerical results and discussions

7.1. Model validations

The capability of the present model to reproduce results from the open literature is carried out herein. Ellipsoidal inclusions are defined by semi-axis (a_1, a_2, a_3) with aspect ratio AR such as $AR = \frac{a_3}{a_1}$ and $a_1 = a_2 = a$. A pure sliding case is considered i.e $\alpha \neq 0$ and $\beta = 0$. The sliding interfacial separation constant α is given such as $\alpha = a\alpha_0/G_M$ with α_0 the sliding coefficient, G_M the shear modulus of the matrix and a the ellipsoid semi-axis. The model predictions are compared with the works by Yanase and Ju [31] on spherical particle-reinforced composites. The material properties used for this study is presented in Table 1.

Matrix		Inclusions			
E_0 [GPa]	ν_0	E_I [GPa]	ν_I	AR	β
3.0	0.4	76	0.23	1.0	0.0

Table 1: Material properties from works by Yanase and Ju [31]

The model predictions are concerned with the originate Mori-Tanaka scheme for perfect bonded inclusions denoted "*MT*" and the modified MT using the modified Eshelby's tensor denoted "*Modif. MT*, $\alpha_0 = 0.3$". Figure 4 presents the influence of the sliding coefficient α_0 on the normalised effective Young modulus E_{eff}/E_0. Under the perfect interface condition, i.e $\alpha_0 = 0$ and beyond a volume fraction $f_I = 0.2$ the MT scheme underestimates results by Yanase and Ju [31]. One can explain this observation by the well-known accuracy issues with the MT when a high volume fraction is achieved. Subsequently, when the interface imperfection is considered with $\alpha_0 = 2.10^{-4}$, a significant decrease of the E_{eff}/E_0 is noticed with respect to the case of perfect interface. However, the effective response show an increase with the volume fraction and good agreement is obtained with results by Yanase and Ju [31]. For high interface damage i.e $\alpha_0 = \infty$,

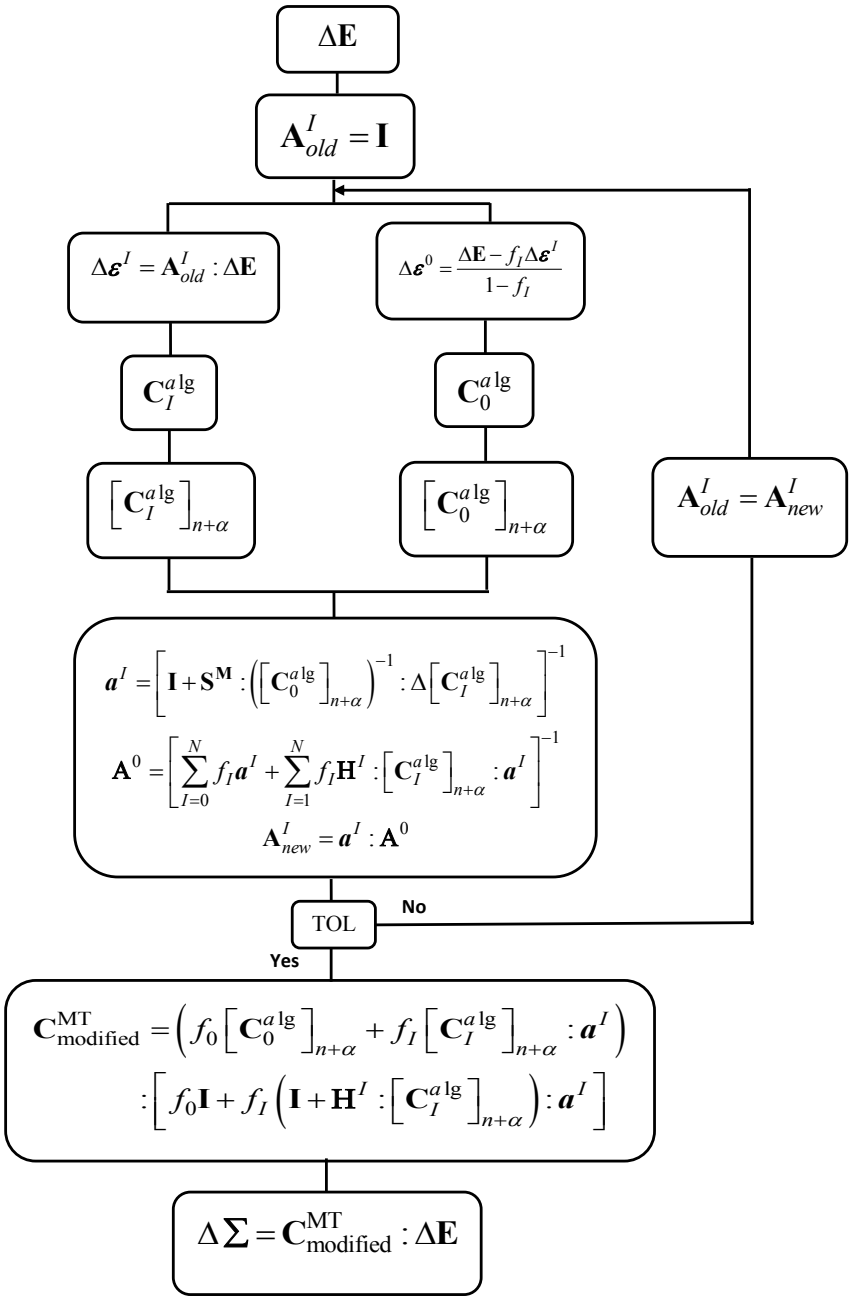

Figure 3: Algorithm for solving the homogenised problem.

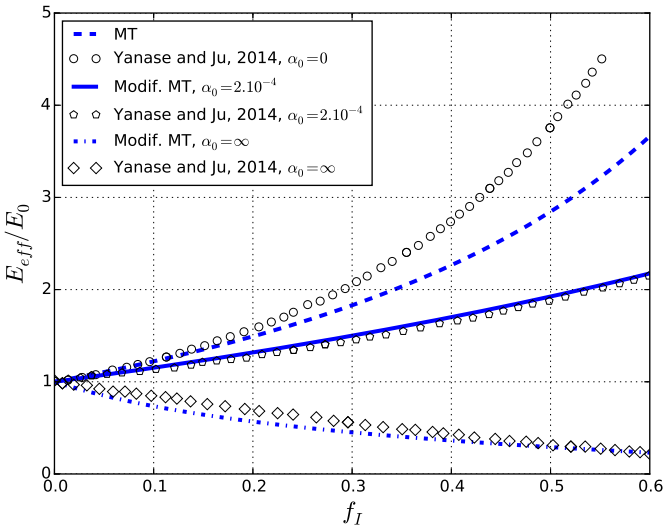

Figure 4: Effective Young modulus of spherical particles reinforced composite.

E_{eff}/E_0 shows a decrease with the volume fraction evolution. Again, the predictions remains in good agreement is obtained with results by Yanase and Ju [31].

7.2. GPL-reinforced polymer PA6 composite materials

Let us consider a composite consisting of GPL reinforced PA-6 ductile polymer matrix. The GPL are assumed elastic while the PA-6 matrix is considered elasto-plastic with an isotropic hardening power law defined as $R(r) = hr^m$. The material properties is presented in Table 2. The macro stress-strain response is studied under uniaxial loading. The loading is given in terms of a macro stain increment $\Delta\mathbf{E} = \Delta E\ \mathbf{\Psi}$ with $\mathbf{\Psi} = \mathbf{e}_1 \otimes \mathbf{e}_1 - \frac{1}{2}(\mathbf{e}_2 \otimes \mathbf{e}_2 + \mathbf{e}_3 \otimes \mathbf{e}_3)$.

Figures 5 and 6 present the behaviours of the matrix under the selected loading. Indeed, figure 5 depicts the accumulated plastic strain p and the variable damage D versus the equivalent deformation. These internal variables are nil during the elastic stage. They increase while the plastic stage is reached. p and D are analysed with respect to the GPL volume fraction f_I. One can remark that during the plastic stage, p and D are sensitive to f_I. The higher, f_I, the higher p and D. However, due to the selected damage evolution law, the value of D remains lower than that of the accumulated plastic strain p. Figure 6 shows the evolution of the strain energy release $\mathbf{Y}$ versus p. constant value of $\mathbf{Y}$ is obtained for the elastic stage i.e $p = 0$. Thereafter, a trend corresponding to a monotonic increase is showed with increasing p leading to a plastic stage. For the whole material behaviour, $\mathbf{Y}$ remains insensitive to the volume fraction f_I.

The effective response of the composite is assessed through different design parameters for

instance the platelets aspect ratio AR, the volume fraction f_I and the interface sliding coefficient α_0.

Matrix							Inclusions	
E_0 [GPa]	ν_0	σ_Y [MPa]	h [MPa]	m	S_0 [MPa]	s	E_I [GPa]	ν_I
2.0	0.39	60.5	63	0.4	2.0	0.5	1000	0.22

Table 2: Material properties for GPL/PA-6 composite materials

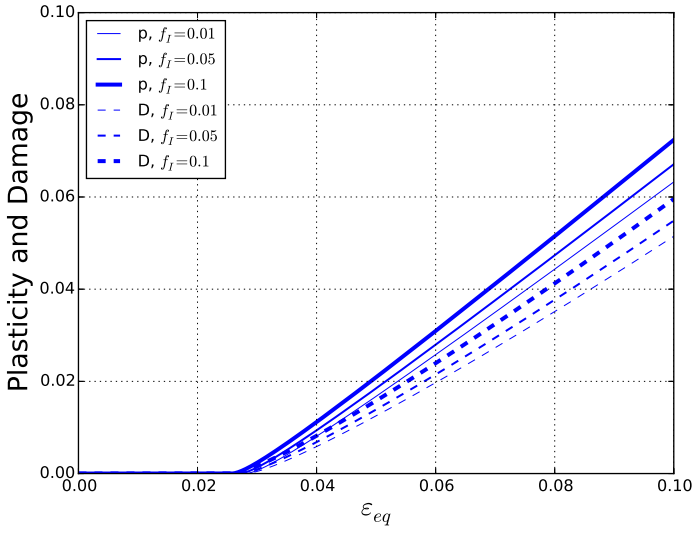

Figure 5: Accumulated plastic strain and damage evolution.

Figure 7 examines the influence of the particle's morphology through AR. The variation of AR on the overall response clearly reproduce the trend of a ductile material starting from the elastic stage to the plastic and damage threshold. The overall response is highly sensitive to the AR. Lower values of AR have led to stiffer stress-strain response. This confirms that the reinforcement character is obtained with platelet-like inclusions $AR < 10^{-1}$ than spherical particles i.e $AR = 1$.

Furthermore, the volume fraction f_I is studied in Figure 8. An increase of the Young modulus, yield strength and hardenning is observed when increasing f_I. In that condition, the composite shifts towards stiff stress-strain response. Figure 9 shows the influence of the interfacial sliding compliance α_0 on the overall response between $\alpha_0 = 0$ corresponding to a perfect interface to $\alpha_0 = 0.7$ representing a delamination. While the Young modulus and yield strength are conserved

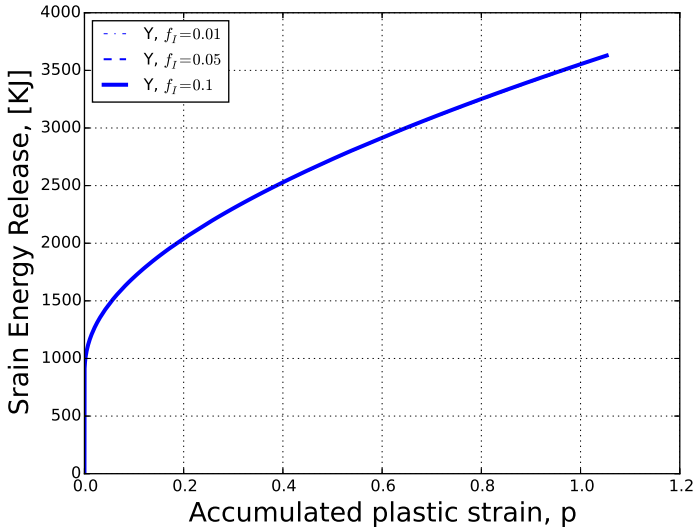

Figure 6: Strain energy release evolution.

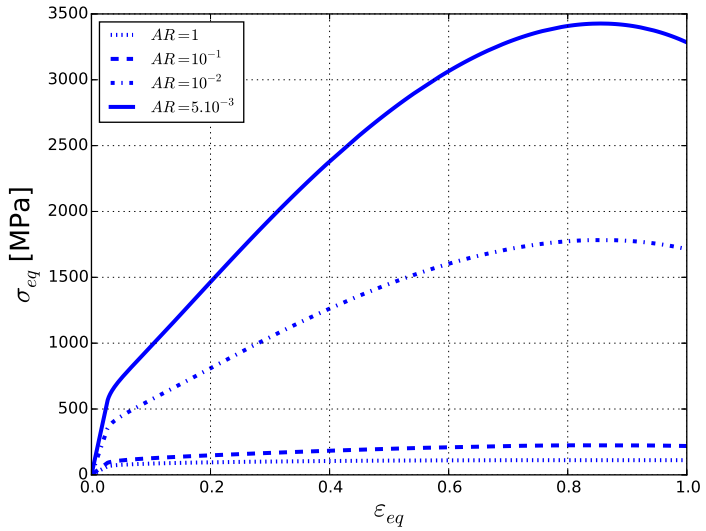

Figure 7: Aspect ratio variation of GPL/PA-6 composite for $f_I = 0.1$ and $\alpha_0 = 0.3$.

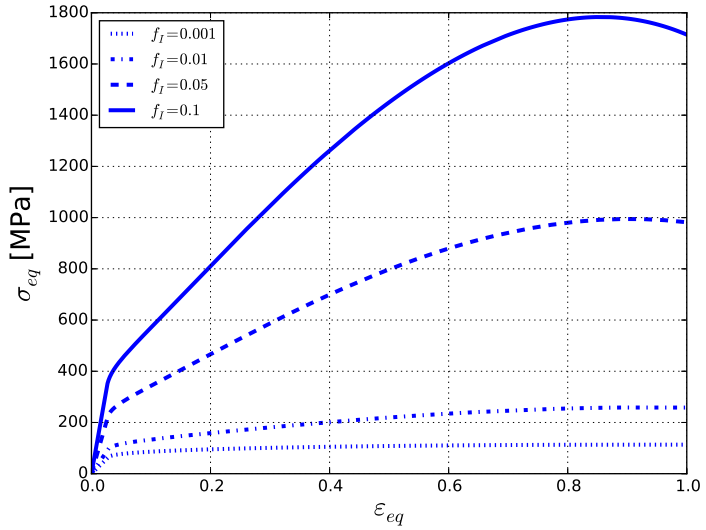

Figure 8: Volume fraction variation of GPL/PA-6 composite for $AR = 10^{-2}$ and $\alpha_0 = 0.3$.

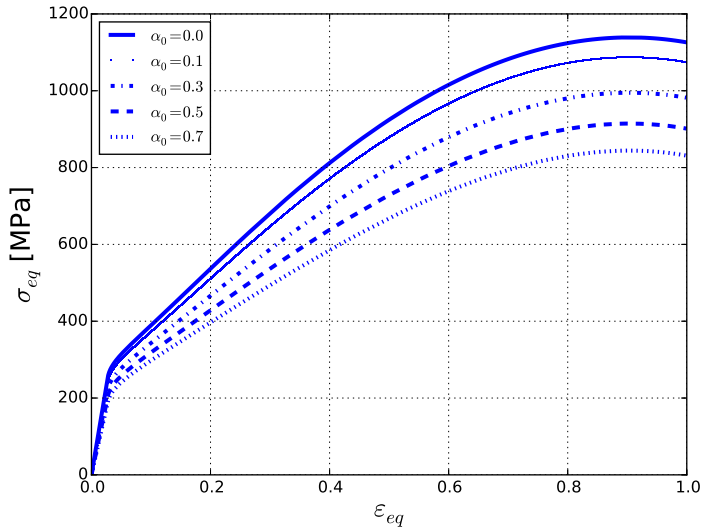

Figure 9: Interface sliding compliance variation of GPL/PA-6 composite for $AR = 10^{-2}$.

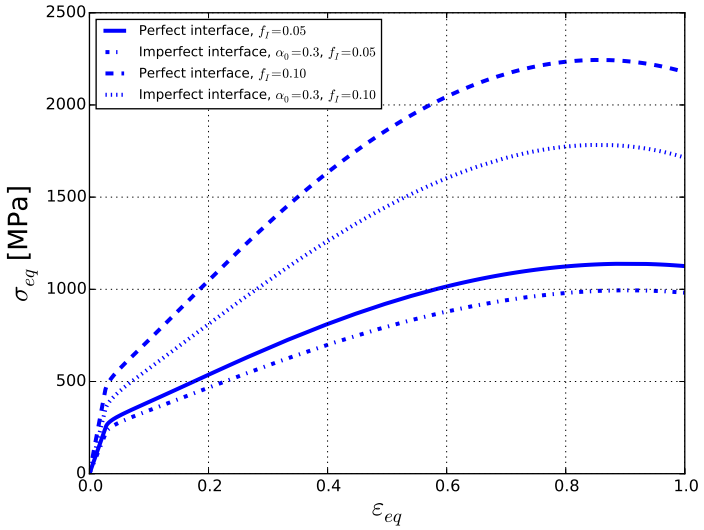

Figure 10: Influence of imperfect versus perfect interface of GPL/PA-6 composite for $AR = 10^{-2}$.

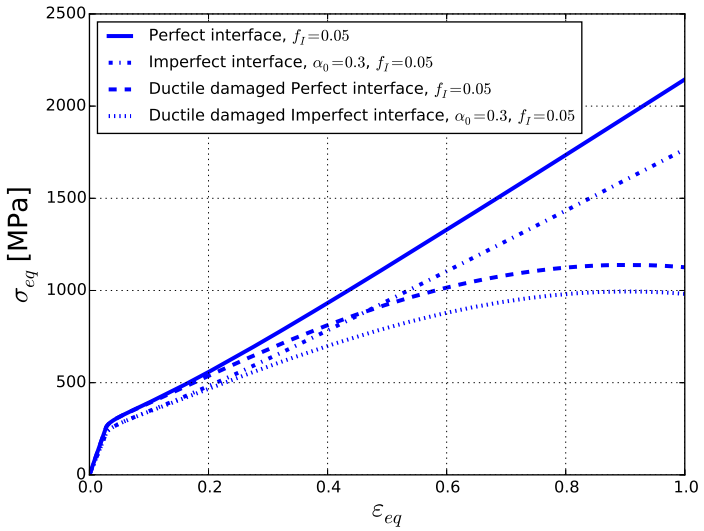

Figure 11: Plasticity versus damage of GPL/PA-6 composite for $AR = 10^{-2}$.

for the composite, the hardening stress decreases when increasing the sliding compliance α_0. The higher, the sliding compliance α_0, the softer the overall response. Comparisons between the composite response in the perfect as well as imperfect interface cases are addressed by figure 10. Two values of volume fraction f_I are considered. While a decrease of the overall response with respect to the imperfect interface case is noticed, the volume fraction f_I shows a significant influence on the increase of the gap between both interfacial cases. In figure 11, the ductile damage behaviour is presented versus the classical plasticity for $f_I = 0.05$. Perfect and imperfect interfaces are analysed and it can be seen a softening in the overall response when damage is accounting for.

8. Conclusion

Graphene platelets reinforced PA-6 polymer composite has been addressed regarding an interfacial behaviour using a micromechanics formulation. For such a purpose, the linear spring model LSM is considered within the framework of Lemaitre-Chaboche model. Therefore, a modified expression is obtained for both the Eshelby's tensor and the Mori-Tanaka scheme for deriving the effective properties that are compared to open literature data. Furthermore, analyses are performed on the ductile matrix internal variables such as the accumulated plastic strain p and damage variable D as well as the strain energy release $\mathbf{Y}$.

Numerical results show that p and D are sensitive to the variation of the GPL volume fraction while $\mathbf{Y}$ remains constant. For the composite, the results highlight the importance of the aspect ratio that leads to most effective reinforcement with low values such as $AR < 10^{-1}$. By considering the interfacial imperfection, the sliding compliance coefficient α_0 also shows a significant influence on the composite overall response and thus, with respect to the GPL the volume fraction. The higher the GPL volume fraction, the higher the softening in the overall stress-stress response.

9. Acknowledgements

The research leading to these results has received funding from the European Union Seventh Framework Programme under grant agreement No. 604391 and Horizon 2020 Programme under grant agreement No. 696656 Graphene Flagship.

Appendix A. Expressions of tensor H

The components of the interfacial tensor $\mathbf{H}$ are given by:

$$H_{ijkl} = \alpha P_{ijkl} + (\beta - \alpha)\, Q_{ijkl} \tag{A.1}$$

where P_{ijkl} and Q_{ijkl} are given for ellipsoidal inclusions by:

$$\begin{cases} P_{ijkl} = \frac{3}{16\pi}\int_0^{\pi}\left[\int_0^{2\pi}\left(\delta_{ik}n_jn_l + \delta_{jk}n_in_l + \delta_{il}n_kn_j + \delta_{jl}n_kn_i\right)\mathbf{n}^{-1}d\theta\right] sin\phi d\phi \\ Q_{ijkl} = \frac{3}{4\pi}\int_0^{\pi}\left[\int_0^{2\pi}\left(n_in_jn_kn_l\right)\mathbf{n}^{-3}d\theta\right] sin\phi d\phi \\ \mathbf{n} = \left(n_in_i\right)^{1/2} \\ n = \left(\frac{sin\phi cos\theta}{a_1}; \frac{sin\phi sin\theta}{a_2}; \frac{cos\theta}{a_3}\right)^{\mathbf{T}} \end{cases} \tag{A.2}$$

References

[1] T. Kuilla, S. Bhadra, D. Yao, N. H. Kim, S. Bose, J. H. Lee, Recent advances in graphene based polymer composites, Progress in Polymer Science 35 (11) (2010) 1350 – 1375. doi:http://dx.doi.org/10.1016/j.progpolymsci.2010.07.005.

[2] R. Barretta, L. Feo, R. Luciano, F. M. de Sciarra, Application of an enhanced version of the eringen differential model to nanotechnology, Composites Part B: Engineering 96 (2016) 274 – 280. doi:http://dx.doi.org/10.1016/j.compositesb.2016.04.023.

[3] J. Xiao, B. Gama, J. G. Jr., An analytical molecular structural mechanics model for the mechanical properties of carbon nanotubes, International Journal of Solids and Structures 42 (2005) 3075 – 3092. doi:http://dx.doi.org/10.1016/j.ijsolstr.2004.10.031.

[4] J. Cho, J. Luo, I. Daniel, Mechanical characterization of graphite/epoxy nanocomposites by multi-scale analysis, Composites Science and Technology 67 (1112) (2007) 2399 – 2407. doi:http://dx.doi.org/10.1016/j.compscitech.2007.01.006.

[5] M. A. Rafiee, J. Rafiee, I. Srivastava, Z. Wang, H. Song, Z.-Z. Yu, N. Koratkar, Fracture and fatigue in graphene nanocomposites, Small 6 (2) (2010) 179–183. doi:10.1002/smll.200901480.

[6] L. M. Veca, M. J. Meziani, W. Wang, X. Wang, F. Lu, P. Zhang, Y. Lin, R. Fee, J. W. Connell, Y.-P. Sun, Carbon nanosheets for polymeric nanocomposites with high thermal conductivity, Advanced Materials 21 (20) (2009) 2088–2092. doi:10.1002/adma.200802317.

[7] Z. Xu, C. Gao, In situ polymerization approach to graphene-reinforced nylon-6 composites, Macromolecules 43 (16) (2010) 6716–6723. doi:10.1021/ma1009337.

[8] W. L. Zhang, B. J. Park, H. J. Choi, Colloidal graphene oxide/polyaniline nanocomposite and its electrorheology, Chem. Commun. 46 (2010) 5596–5598. doi:10.1039/C0CC00557F.

[9] L.-J. Walpole, A coated inclusion in an elastic medium, Mathematical Proceedings of the Cambridge Philosophical Society 83 (1978) 495. doi:10.1017/S0305004100054773.

[10] R. M. Christensen, K. H. Lo, Solutions for effective shear properties in three phase sphere and cylinder models, Journal of the Mechanics and Physics of Solids 27 (4) (1979) 315 – 330. doi:DOI:10.1016/0022-5096(79)90032-2.

[11] E. Hervé, A. Zaoui, n-layered inclusion-based micromechanical modelling, International Journal of Engineering Science 31 (1) (1993) 1 – 10. doi:DOI:10.1016/0020-7225(93)90059-4.

[12] M. Cherkaoui, H. Sabar, M. Berveiller, Micromechanical approach of the coated inclusion problem and applications to composite materials, Journal of engineering materials and technology, vol. 116, no 3 (11 ref.), pp. 274-278 (1994).

[13] P. Lipinski, E. Barhdadi, M. Cherkaoui, Micromechanical modeling of an arbitrary ellipsoidal multi-coated inclusion, Philosophical Magazine 86 (10) (2006) 1305–1326.

[14] K. Matous, P. H. Geubelle, Finite element formulation for modeling particle debonding in reinforced elastomers subjected to finite deformations, Computer Methods in Applied Mechanics and Engineering 196 (1-3) (2006) 620 – 633. doi:DOI:10.1016/j.cma.2006.06.008.

[15] H. Inglis, P. Geubelle, K. Matous, H. Tan, Y. Huang, Cohesive modeling of dewetting in particulate composites: micromechanics vs. multiscale finite element analysis, Mechanics of Materials 39 (6) (2007) 580 – 595. doi:http://dx.doi.org/10.1016/j.mechmat.2006.08.008.

[16] H. Tan, Y. Huang, C. Liu, P. Geubelle, The mori-tanaka method for composite materials with nonlinear interface debonding, International Journal of Plasticity 21 (10) (2005) 1890 – 1918. doi:DOI:10.1016/j.ijplas.2004.10.001.

[17] H. Tan, C. Liu, Y. Huang, P. Geubelle, The cohesive law for the particle/matrix interfaces in high explosives, Journal of the Mechanics and Physics of Solids 53 (8) (2005) 1892 – 1917. doi:http://dx.doi.org/10.1016/j.jmps.2005.01.009.

[18] F. Ghahremani, Effect of grain boundary sliding on anelasticity of polycrystals, International Journal of Solids and Structures 16 (9) (1980) 825 – 845. doi:http://dx.doi.org/10.1016/0020-7683(80)90052-9.

[19] P. Sharma, S. Ganti, N. Bhate, Effect of surfaces on the size-dependent elastic state of nano-inhomogeneities, Appl. Phys. Lett 82 (2003) 535.

[20] P. Sharma, S. Ganti, Size-dependent eshelby's tensor for embedded nano-Inclusions incorporating surface/interface energies, journal of applied mechanics (2004).

[21] P. Sharma, L. T. Wheeler, Size-dependent elastic state of ellipsoidal nano-inclusions incorporating surface/interface tension, Journal of Applied Mechanics Vol. 74 (2007) 447.

[22] H. Duan, J. Wang, Z. Huang, B. Karihaloo, Eshelby formalism for nano-inhomogeneities, Proc. R. Soc. A 461 (2005) 3335–3353.

[23] H. Duan, J. Wang, Z. Huang, B. Karihaloo, Size-dependent effective elastic constants of solids containing nano-inhomogeneities with interface stress, Journal of the Mechanics and Physics of Solids 53 (7) (2005) 1574 – 1596. doi:DOI:10.1016/j.jmps.2005.02.009.

[24] Z. Hashin, The spherical inclusion with imperfect interface, Journal of Applied Mechanics 58 (2) (1991) 444–449. doi:10.1115/1.2897205.

[25] Z. Hashin, Thermoelastic properties of particulate composites with imperfect interface, Journal of the Mechanics and Physics of Solids 39 (6) (1991) 745 – 762. doi:http://dx.doi.org/10.1016/0022-5096(91)90023-H.

[26] J. Qu, The effect of slightly weakened interfaces on the overall elastic properties of composite materials, Mechanics of Materials 14 (4) (1993) 269 – 281. doi:http://dx.doi.org/10.1016/0167-6636(93)90082-3.

[27] J. Qu, Eshelby tensor for an elastic inclusion with slightly weakened interface, Journal of Applied Mechanics 60 (4) (1993) 1048–1050. doi:10.1115/1.2900974.

[28] Z. Zhong, S. A. Meguid, On the elastic field of a shpherical inhomogeneity with an imperfectly bonded interface, Journal of Elasticity 46 (2) (1997) 91–113. doi:10.1023/A:1007342605107.

[29] G. Mancusi, L. Feo, V. P. Berardi, Concrete open-wall systems wrapped with frp under torsional loads, Materials 5 (11) (2012) 2055. doi:10.3390/ma5112055.

[30] L. Ascione, V. Berardi, L. Feo, G. Mancusi, A numerical evaluation of the interlaminar stress state in externally {FRP} plated {RC} beams, Composites Part B: Engineering 36 (1) (2005) 83 – 90. doi:http://dx.doi.org/10.1016/S1359-8368(03)00018-0.

[31] K. Yanase, J. Ju, Overall elastoplastic damage responses of spherical particle-reinforced composites containing imperfect interfaces, International Journal of Damage Mechanics vol. 23 (no. 3) (2014) 411–429.

[32] P. H. Dederichs, R. Zeller, Variational treatment of the elastic constants of disordered materials, Zeitschrift fur Physik A Hadrons and Nuclei Volume 259, Number 2, 103-116, DOI: 10.1007/BF01392841.

[33] A. Tchalla, W. Azoti, Y. Koutsawa, A. Makradi, S. Belouettar, H. Zahrouni, Incremental mean-fields micromechanics scheme for non-linear response of ductile damaged composite materials, Composites Part B: Engineering 69 (0) (2015) 169 – 180. doi:http://dx.doi.org/10.1016/j.compositesb.2014.08.055.

[34] I. Doghri, Mechanics of deformable solids, Linear and nonlinear, analytical and computational aspects, Springer-Verlag, 2000.

[35] L. Wu, L. Noels, L. Adam, I. Doghri, A multiscale mean-field homogenization method for fiber-reinforced composites with gradient-enhanced damage models, Computer Methods in Applied Mechanics and Engineering 233 - 236 (0) (2012) 164 – 179. doi:http://dx.doi.org/10.1016/j.cma.2012.04.011.

[36] L. Wu, L. Noels, L. Adam, I. Doghri, An implicit-gradient-enhanced incremental-secant mean-field homogenization scheme for elasto-plastic composites with damage, International Journal of Solids and Structures 50 (24) (2013) 3843 – 3860. doi:http://dx.doi.org/10.1016/j.ijsolstr.2013.07.022.

[37] R. Barretta, L. Feo, R. Luciano, F. M. de Sciarra, R. Penna, Functionally graded timoshenko nanobeams: A novel nonlocal gradient formulation, Composites Part B: Engineering 100 (2016) 208 – 219. doi:http://dx.doi.org/10.1016/j.compositesb.2016.05.052.

[38] A. Apuzzo, R. Barretta, M. Canadija, L. Feo, R. Luciano, F. M. de Sciarra, A closed-form model for torsion of nanobeams with an enhanced nonlocal formulation, Composites Part B: Engineering 108 (2017) 315 – 324. doi:http://dx.doi.org/10.1016/j.compositesb.2016.09.012.

[39] R. Barretta, R. Luciano, J. R. Willis, On torsion of random composite beams, Composite Structures 132 (2015) 915 – 922. doi:http://dx.doi.org/10.1016/j.compstruct.2015.06.069.

[40] I. Doghri, A. Ouaar, Homogenization of two-phase elasto-plastic composite materials and structures: Study of tangent operators, cyclic plasticity and numerical algorithms, International Journal of Solids and Structures 40 (7) (2003) 1681 – 1712. doi:10.1016/S0020-7683(03)00013-1.

[41] J. Chaboche, P. Kanoute, A. Roos, On the capabilities of mean-field approaches for the description of plasticity in metal matrix composites, International Journal of Plasticity 21 (7) (2005) 1409 – 1434. doi:http://dx.doi.org/10.1016/j.ijplas.2004.07.001.

[42] P. Vieville, A. S. Bonnet, P. Lipinski, Modelling effective properties of composite materials using the inclusion concept. general considerations, Arch. Mech. 58 (3) (2006) 207–239.

[43] O. Fassi-Fehri, Le problème de la paire d'inclusions plastiques et hétérogènes dans une matrice anisotrope : Application à l'étude du comportement des matériaux composites et de la plasticité, Ph.D. thesis, Université de Metz (1985).

[44] J. D. Eshelby, The determination of the elastic field of an ellipsoidal inclusion, and related problems, Proceedings of the Royal Society of London. Series A, Mathematical and Physical Sciences 241 (1226) (1957) 376–396.

[45] W. Azoti, A. Tchalla, Y. Koutsawa, A. Makradi, G. Rauchs, S. Belouettar, H. Zahrouni, Mean-field constitutive modeling of elasto-plastic composites using two (2) incremental formulations, Composite Structures 105 (2013) 256–262. doi:10.1016/j.compstruct.2013.05.044.

[46] W. Azoti, Y. Koutsawa, A. Tchalla, A. Makradi, S. Belouettar, Micromechanics-based multi-site modeling of elastoplastic behavior of composite materi-

als, International Journal of Solids and Structures 59 (2015) 198 – 207. doi:http://dx.doi.org/10.1016/j.ijsolstr.2015.02.002.

Research Highlights

- The graphene platelets GPL are defined through the aspect ratio of inclusions;
- The non linear behaviour is based on the Lemaitre-Chaboche damage model;
- The linear spring model is used for studying the interfacial imperfection;
- The overall properties are derived by a modified Mori-Tanaka scheme;
- Numerical results are carried out for GPL reinforced polymer under uniaxial loading.